

# High-temperature oxidation resistance of Ti-implanted E110 alloy

E B Kashkarov, M S Syrtanov, A E Shevelev, A V Kurochkin and S K Pavlov

National Research Tomsk Polytechnic University, 634050 Tomsk, Russia

E-mail: egor\_kashkarov@mail.ru

**Abstract.** This paper describes the effect of surface modification by high-intensity Ti-ion implantation on the high-temperature oxidation resistance of E110 zirconium alloy. The oxidation tests were performed in air at 873 K for 10 h and in water steam at 1373 K for 10 min. The microstructure, phase composition and depth distribution of elements were analysed using scanning electron microscopy, X-ray diffraction and glow-discharge optical emission spectroscopy, respectively.

## 1. Introduction

The accident at the Fukushima Daiichi power plant occurred in 2011 gave impetus to international research on the development of protective coatings for nuclear cladding tubes [1]. Besides zirconium claddings are resistant to corrosion and oxidation under the normal operating temperature, they cannot ensure the protection of light-water reactors under loss-of-coolant accident (LOCA) conditions. The accelerated corrosion reaction in water steam at 1373-1473 K leads to generation of explosive hydrogen and degradation of mechanical properties of nuclear fuel claddings. Currently, the deposition of protective coatings such as Cr, SiC, CrN, TiN/TiAlN and other are being developed to increase oxidation resistance of zirconium alloy [2–5]. However, the adhesion properties of protective coatings are the weaknesses of coating technology; therefore, surface modification by charged particle beams has also been developed. A high-intensity implantation of low-energy titanium ions can be implemented to form a deep modified layer providing enhanced mechanical and tribological properties of zirconium alloys [6]. However, the oxidation resistance of the Ti-doped surface modified zirconium alloy has not been studied. In the present work, the high-temperature corrosion behavior of E110 zirconium alloy with a surface modified layer formed by high-intensity ion implantation was considered.

## 2. Materials and Methods

### 2.1. Ion implantation

The samples with the size of 20×20×2 mm were cut from a cold rolled E110 (Zr–1Nb) zirconium alloy. The samples were grinded using a SiC abrasive paper and ultrasonically cleaned in acetone for 15 min. For surface modification, a high-intensity beam of low-energy Ti ions was used. To generate the direct current (DC) flow of metal plasma a vacuum arc evaporation system was used. The high-current density of metal ions was provided by the hemispherical ballistic focusing system. The ion beam formation, transportation and ballistic focusing system were described in [7]. The implantation parameters are



shown in Table 1. According to energy-dispersive spectroscopy, the titanium has a gradient distribution up to 10  $\mu\text{m}$  in depth with the maximum concentration of 55 at.% in the surface [8].

**Table 1.** Ion implantation parameters

Ion current density	Pulse duration	Duty factor	Temperature	Fluence
100 mA/cm <sup>2</sup>	5 $\mu\text{s}$	0.5	973 K	5.6 $\times 10^{20}$ ion/cm <sup>2</sup>

### 2.2. High-temperature oxidation and characterization

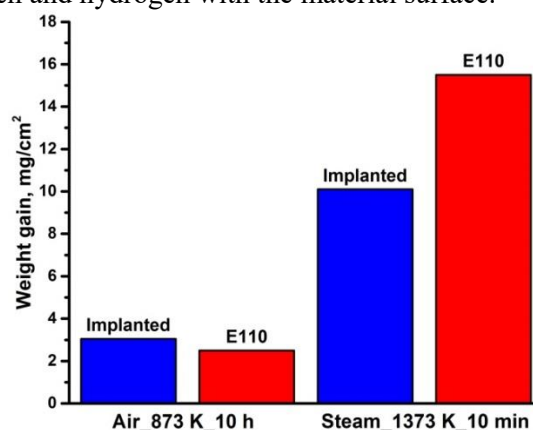
High temperature oxidation tests were performed in air atmosphere at 873 K for 10 h and in steam at 1373 K for 10 min. For the oxidation tests, the samples were placed in pre-heated chambers. For the steam oxidation test a furnace with evaporation equipment was used. The temperature was controlled by a thermocouple. After the oxidation tests, the weight gains were measured using analytical weighing-machine (Sartorius CP124 S) with an accuracy of  $10^{-4}$  g. The samples after steam oxidation test were quenched in water from approximately 1073 K.

The phase composition was analyzed by X-ray diffraction ( $\text{CuK}\alpha$  radiation) using XRD 7000S diffractometer (Shimadzu, Japan) equipped with 1280-channel high-speed detector OneSight. The acceleration voltage and current were 40 kV and 30 mA, respectively. The diffraction data was analyzed using Sleve+ program and ICDD PDF-4+ database. The microstructure was analyzed by scanning electron microscopy (SEM) using S-2400N (Hitachi, Japan). For microstructural analysis, the samples were chemically etched in a solution of 45%  $\text{HNO}_3$ , 5% HF and 50 %  $\text{H}_2\text{O}$ .

## 3. Results and discussion

### 3.1. Weight gain

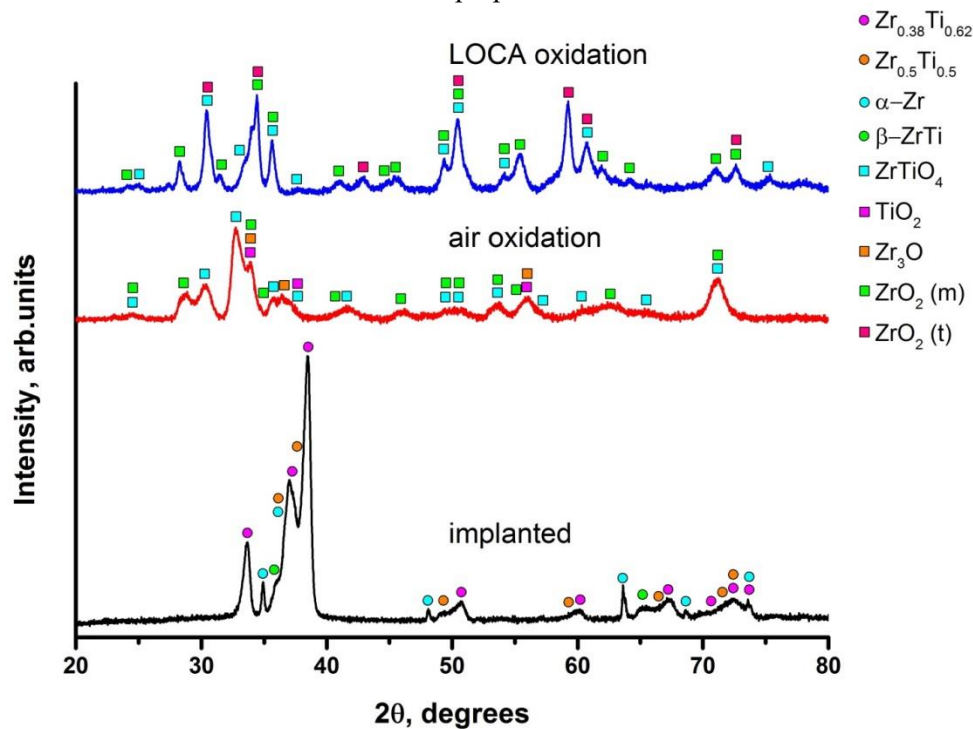
The samples were oxidized in atmosphere at 873 K to analyse the heat-resistance of the Ti-implanted alloy. The steam oxidation test was performed to evaluate the high-temperature resistance of the implanted alloy under the conditions simulating LOCA. Therefore, the weight gains of the surface modified samples were measured and compared with that of the untreated E110 alloy (Figure 1). It was found that the high-temperature oxidation resistance of the implanted sample depends on the oxidation conditions. After the oxidation in air, the weight gain of the surface-modified sample is higher by 20% in comparison with the E110 alloy. It indicates degradation of the oxidation resistance properties of zirconium alloy. On the contrary, the oxidation of the Ti-implanted alloy in steam is significantly lower than that of the untreated alloy. Such difference may be attributed to the specificity of the oxidation mechanisms as well as the difference in oxidation temperature. The presence of nitrogen during air oxidation of the modified layer can accelerate the oxidation process due to partial replacement of oxygen atoms in titanium and zirconium oxides. In turn, during the oxidation in stream, the main role is related to the interaction of oxygen and hydrogen with the material surface.



**Figure 1.** The weight gains of the samples after high-temperature oxidation in air and steam.

### 3.2. Phase composition

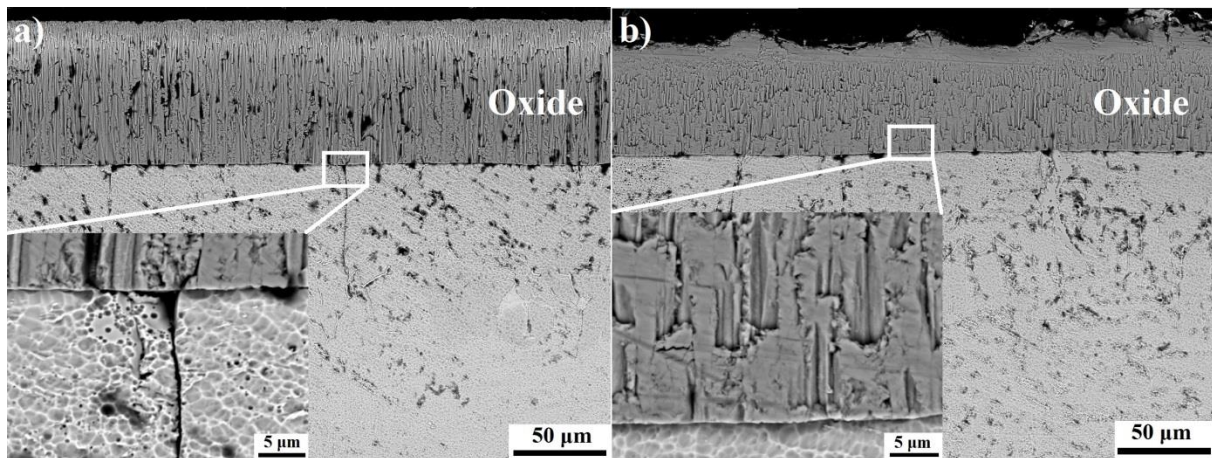
Figure 2 shows the diffraction patterns of Ti-implanted zirconium alloy after oxidation. According to X-ray analysis the as-implanted alloy consist of Zr-Ti solid solution ( $Zr_{0.38}Ti_{0.62}$ ,  $Zr_{0.5}Ti_{0.5}$ ),  $\alpha$ -Zr phases with hcp structure and  $\beta$ -Zr phase with fcc structure. The phase composition of Ti-implanted zirconium alloy significantly changes after oxidation. The oxidation in air at 873 K for 10 h leads to the formation of monoclinic  $ZrO_2$ , hexagonal  $Zr_3O$ , hexagonal  $TiO_2$  and orthorhombic  $ZrTiO_4$  phases. The formation of orthorhombic  $ZrTiO_4$  phase at slightly milder oxidation conditions was also observed in [9]. As a result of LOCA oxidation tests, in addition to monoclinic  $ZrO_2$  and orthorhombic  $ZrTiO_4$  phases, the tetragonal  $ZrO_2$  phase was detected. It should be noted that the oxidation conditions directly affect the phase composition of Ti-implanted zirconium alloy. Moreover, the analysis of the diffraction patterns indicates the changes in oxides phase content depending on oxidation conditions. However, it is difficult to calculate the exact values of content due to superposition of its reflections.



**Figure 2.** Diffraction patterns of Ti-implanted zirconium alloy after oxidation tests.

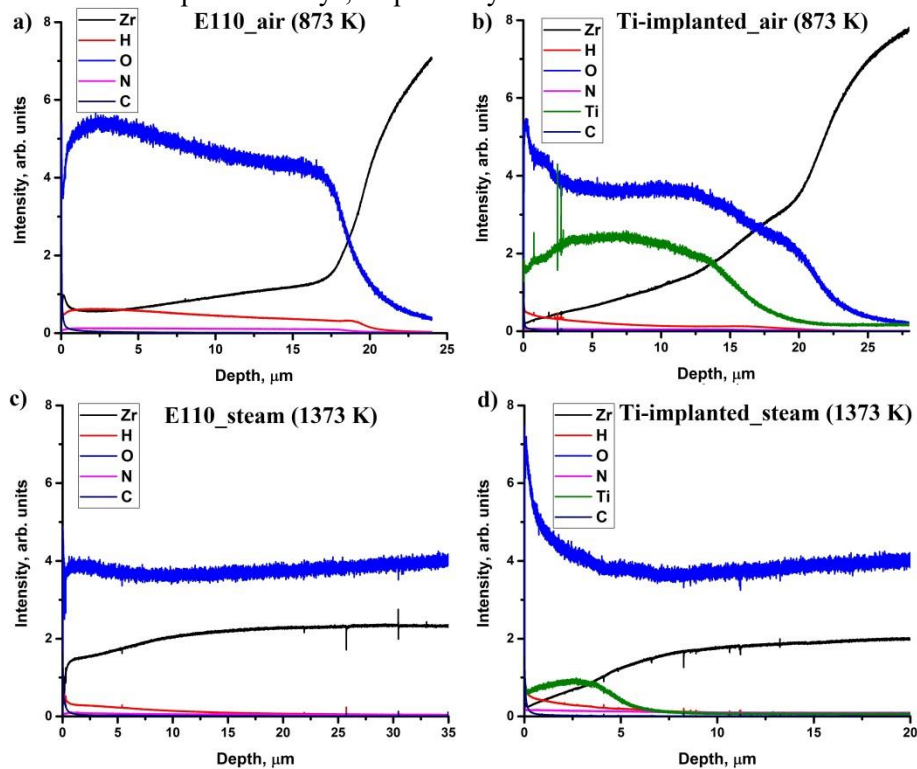
### 3.3. Microstructure and elemental distribution

Figure 3 shows the microstructure of the formed oxides after high-temperature oxidation test at 1373 K. The oxides have a columnar structure grown perpendicular to the alloy surface. The formation of high amount of cracks at the oxide/metal interface was observed in the oxidized E110 alloy. The propagation of these cracks apparently occurs across the grain boundaries of the primary  $\beta$  phase due to relaxation of tensile/compressive stresses at the oxide/metal interface. It should be noted that an oxygen-oversaturated solid solution  $\alpha$ -Zr(O) forms under the oxide layer, which have a lamellar microstructure formed due to  $\beta \rightarrow \alpha$  phase transformations during rapid cooling from the  $\beta$  phase. The thickness of the oxide layer in Ti-implanted sample is lower than that of the E110 alloy. It well correlates with the measured weight gain data. Although small microcracks have been found at the metal/oxide interface in the implanted sample, this interface is fairly uniform and has the dense microstructure. It is also seen a non-uniform corrosion in the upper oxide layer, but it has a denser structure that apparently decrease the diffusion of oxygen and enhances the corrosion resistance.



**Figure 3.** Cross-section SEM images of the steam oxidized E110 (a) and Ti-implanted E110 (b).

Figure 4 shows the depth distribution of elements in the oxidized samples. After oxidation in air, the thickness of the oxide layer was  $\sim 18 \mu\text{m}$  and  $\sim 22 \mu\text{m}$  for the untreated and Ti-implanted samples, which is in good agreement with the SEM data (not shown in the article). In both cases, the oxide compounds with porous microstructure are formed. It is also seen that the thickness of the formed oxide layer exceeds the thickness of the Ti-modified layer ( $\sim 10 \mu\text{m}$ ), which leads to the formation of  $\text{ZrO}_2$  phases under  $\text{TiZrO}_4$  oxide layer. The analysis of glow-discharge optical emission spectroscopy (GDOES) data indicates a partial diffusion of titanium into the alloy depth, especially during oxidation in steam. In the samples oxidized in steam, a thick oxide layer is formed with a fairly uniform distribution of oxygen over the depth. According to SEM results, the thickness of the oxide layer was  $76\text{--}79 \mu\text{m}$  and  $60\text{--}70 \mu\text{m}$  for the untreated and Ti-implanted alloys, respectively.



**Figure 4.** GDOES depth distribution profiles of elements in the oxidized samples.

#### 4. Conclusion

The high-temperature oxidation resistance of E110 zirconium alloy surface modified by high-intensity implantation of low-energy Ti ions was investigated. The oxidation tests have shown the difference in oxidation kinetics of Ti-implanted alloy in air and steam. The corrosion resistance of the implanted alloy during oxidation in air atmosphere is significantly lower than that of the as-received E110 alloy. At the same time, an increase in the high-temperature oxidation resistance of the alloy was observed under LOCA oxidation test, where the weight gain was reduced to 10.1 mg/cm<sup>2</sup>. The formation of orthorhombic TiZrO<sub>4</sub> oxide phase occurs in the implanted layer during oxidation in steam, which has a denser microstructure compared to ZrO<sub>2</sub> oxides. After rapid cooling of the samples after LOCA test, numerous cracks appeared at the oxide/metal interface in the untreated E110 alloy. The oxide layer in the implanted sample has a non-uniform structure on the surface, and there are practically no cracks at the oxide/metal interface. However, the relatively high oxidation rate of the surface Ti-doped alloy does not allow it to be considered as protective layer for fuel cladding.

#### Acknowledgements

The reported research was funded by the Russian Foundation for Basic Research and the government of the Tomsk region of the Russian Federation, grant No. 18-48-703034.

The authors are grateful to Y. Shanenkova for SEM measurements.

#### References

- [1] Minin N 2018 *Energy Strategy Rev.* **21** 98
- [2] Kashkarov E B, Syrtanov M S, Murashkina T L, Kurochkin A V, Shanenkova Y and Obrosov 2019 *Coatings* **9** (1) 31
- [3] Sidelev D V, Kashkarov E B, Syrtanov M S and Krivobokov V P 2019 *Surf. Coat. Technol.* **369** 69
- [4] Tang C, Stueber M, Seifert HJ and Steinbrueck M 2017 *Corros. Rev.* **35** 141
- [5] Duan Z, Yang H, Satoh Y, Murakami K, Kano S, Zhao Z, Shen J and Abe H 2017 *Nucl. Energy Des.* **316** 131
- [6] Ryabchikov A I, Kashkarov E B, Pushilina N S, Syrtanov M S, Shevelev A E, Korneva O S, Sutygina A N and Lider A M 2018 *Appl. Surf. Sci.* **439** 106
- [7] Ryabchikov A I, Ananin P S, Dektyarev S V, Sivin D O and Shevelev A E 2017 *Vacuum* **143** 447
- [8] Kashkarov E B, Ryabchikov A I, Kurochkin A V, Syrtanov M S, Shevelev A E, Obrosov A and Weiß S 2018 *Metals* **8** (12) 1081
- [9] Cui W F and Shao C J 2015 *Surf. Coat. Technol.* **283** 101